JOURNAL OF MATERIALS SCIENCE 30 (1995) 75–84

Thermoelastic stresses in ribbons and tubes grown from the melt by the Stepanov method

A. V. ZHDANOV, L. P. NIKOLAEVA, S. N. ROSSOLENKO
Institute of Solid State Physics, Russian Academy of Sciences, 142432 Chernogolovka, Moscow district, Russia

Ribbons and tubes grown from the melt by the Stepanov technique have a wide range of technical applications. Sapphire ribbons are used as substrates in microelectronics and sapphire tubes are used as gas-discharge balloons in laser engineering, fine chemical technology and high-vacuum equipment. Practice has shown that misorientation angles of small-angle boundaries in sapphire crystals should not exceed several degrees because an increase in the misorientation angles between blocks drastically lowers the strength and worsens the dielectric properties of these crystals. One of the main mechanisms of formation of the block structure of melt-grown crystals, including shaped sapphire crystals, is dislocation polygonization that begins when the dislocation density exceeds a certain critical value. In turn, dislocations are formed under deformations due to thermal stresses. Calculations of thermal fields in crystals and the corresponding thermoelastic stress fields can be used as an input to improve and optimize the growth process. The dependence of thermoelastic stresses in ribbons and tubes on the technological parameters has been calculated.

Nomenclature

α_1	Thermal diffusivity of the melt
α_2	Thermal diffusivity of the crystal
k_1	Thermal conductivity of the melt
k_2	Thermal conductivity of the crystal
V_1	Velocity vector of the melt
V_2	Velocity vector of the growing crystal
V_0	Crystal pulling rate
ΔH_f	Latent heat of fusion
ρ_1	Density of the melt
ρ_2	Density of the crystal
$\boldsymbol{n}$	Interface normal vector
τ	Crystal–melt interface normal vector
t	Interface tangential vector
s	Sided crystal–melt tangential vector
T_m	Melting temperature
T_e	Ambient temperature
T_1^0	Temperature at the bottom of the meniscus
T_2^0	Crystal temperature at the top of the meniscus
τ	Normal vector at lateral surfaces of the crystal and meniscus
σ	Stefan–Boltzmann constant
ε_1	Emissivity of the meniscus lateral surface
ε_2	Emissivity of the crystal lateral surface
g	Acceleration due to gravity
σ_{LG}	Melt–gas surface tension
a	Die half dimension
ϕ_0	Angle of growth
α_t	Thermal expansion coefficient
h_1	Heat transfer coefficient of the melt
h_2	Heat transfer coefficient of the crystal
$c_{\rho s}$	Heat capacity
E	Young's modulus
ν	Poisson's coefficient
μ	Melt kinematic viscosity
P	Pressure in the melt

1. Introduction

Ribbons and tubes grown from the melt by the Stepanov technique have a wide range of technical applications. In particular, sapphire ribbons are used as substrates in microelectronics and sapphire tubes are used as gas-discharge balloons in laser engineering, fine chemical technology and high-vacuum equipment. Practice has shown that misorientation angles of small-angle boundaries in sapphire crystals should not exceed several degrees because an increase in the misorientation angles between blocks drastically lowers the strength and worsens the dielectric properties of these crystals. One of the main mechanisms of formation of the block structure of melt-grown crystals, including shaped sapphire crystals, is dislocation polygonization that begins when the dislocation density exceeds a certain critical value [1, 2]. In turn, dislocations are formed under deformations due to thermal stresses [3–5]. Calculations of thermal fields in crystals and the corresponding thermoelastic stress fields can be used as an input to improve and optimize the growth process [6]. Empirical models of high-temperature inelastic deformation of a crystal during shaped growth from the melt have been developed

0022–2461 © *1995 Chapman & Hall*

recently [7]. However, such models require complicated simulations and powerful computers. In the present work, thermoelastic stresses in crystals as a function of the technological parameters have been calculated.

For the ribbons, a two-dimensional problem of thermoelasticity is solved with allowance for the stresses arising in a crystal when it is growing from the melt. The temperature field is supposed to be independent of the deformations induced. Then the problem can be divided into two stages. The first step is to find the temperature field; it is a Stefan-type problem of phase transition in the melt–crystal system, and consists of finding temperatures for liquid and solid phases, the shape of the interface boundary, the profile curve of the melt meniscus and, finally, the thickness of the growing ribbon.

The *ab initio* numerical solution of this problem includes taking, as an input, the initial thickness, shape and position of interface and thermal field in a crystal and melt. Then, the following iteration procedure is applied.

1. The thermal and velocity fields are determined to solve the heat transfer and Stokes equations and their boundary conditions, by trying various shapes and positions of the interface and crystal thickness.

2. The shape and position of the interface are corrected until the sequence of iterations (1) and (2) converges and yields a temperature on the interface equal to the melting temperature of a material.

3. The ribbon thickness is iterated until the constraint of the constant angle of growth is satisfied.

After the temperature field in the crystal has been found, the corresponding thermoelastic stressed state is determined. The motion of the melt in the capillary and in the meniscus is described by Stokes equations. The resulting differential equations were solved by the finite-element method in the appropriate class of functions.

The analogous problem of thermoelasticity should be considered, and for the case of tubes. Similar Stefan-type and Stokes problems should be solved, but for different geometry. The additional thermal and capillary boundary conditions on the inner crystal-meniscus lateral surface for equations written in a cylindrical coordinate system, have to be introduced. However, this model requires vast computing resources and much computational time. Therefore, we consider a crystal area only with the planar interface. The thickness of tube was determined according to experimental data, namely, by visual observation of the growth process. In addition, the parameters of the growth process, such as pull rate and ambient temperature, were obtained experimentally. The heat exchange of the tube with the environment during growth depends on whether the growing tube is in the screened thermal zone or partially sticks out of this zone beyond a certain length. Both cases have been considered. The case of a semi-infinite tube in the one-dimensional approximation of the temperature field is given [8]. In the present work, we have allowed for the influence of the upper end of the tube, which may be important in determination of the stress distributions. The developed approach allows calculation of the thermoelastic stresses from experimental ambient temperatures along the tube surfaces.

Despite the apparent similarity, we treat the two problems in a somewhat different framework. We would like to emphasize that often it is more effective not to start from scratch, but to proceed from a certain intermediate stage using, as an input, some experimental data. We have already succesfully applied this combined and fruitful approach to different problems.

2. Thermoelastic stresses in ribbons

2.1. Mathematical model

A diagram of the crystallization process and the choice of the coordinate system are illustrated in Fig. 1. Indices 1 and 2 denote the quantities referring to the melt and crystal, respectively. The distribution of temperature $T_1(x, y)$ in the region $D_1 \cup D_2$, involving the melt in the meniscus and the crystal, is described by the thermal conduction equation

$$\alpha_i \Delta T_i = (V_i \cdot \nabla T_i) \quad (x, y) \in D_i, \quad i = 1, 2 \qquad (1)$$

where Δ is the Laplace operator and ∇ is a gradient operator. At the interface $H(x)$, the Stefan condition should be fulfilled

$$k_1(n \cdot \nabla T_1) - k_2(n \cdot \nabla T_2) = \rho_2 V_{0\Delta} H_f (1 + H_x'^2)^{-1/2} \qquad (2a)$$

$$T_1[x, H(x)] = T_2[x, H(x)] = T_m \qquad (2b)$$

$$-b \leqslant x \leqslant b, \quad y = H(x)$$

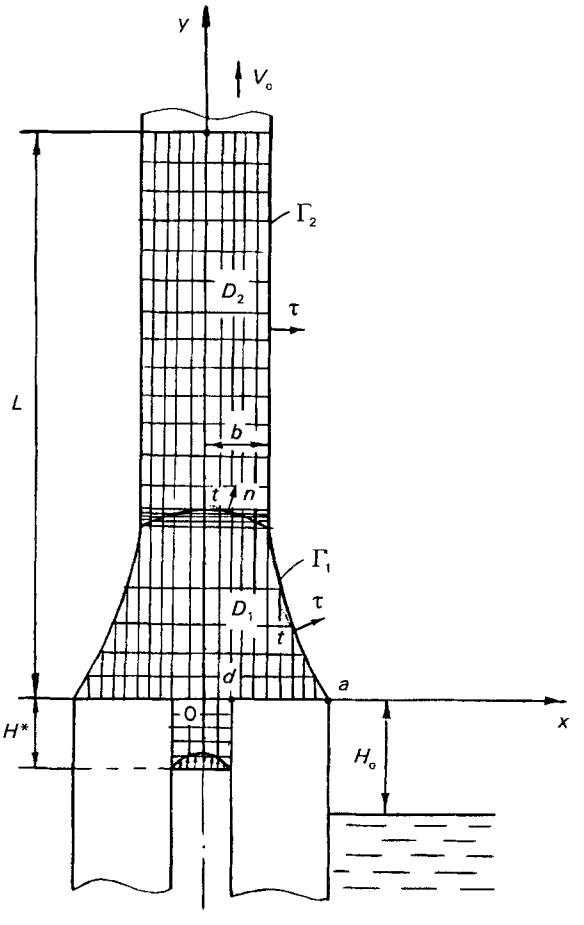

Figure 1 A diagram of ribbon growth and the grid of the finite-element method.

Heat transfer from the melt and crystal to the neighbouring medium at temperature $T_e(y)$, which depends on the height only, is accomplished by convection and radiation

$$-k_i \frac{\partial T_i}{\partial \tau} = h_i(T_i - T_e) + \sigma\varepsilon_i(T_i^4 - T_e^4), \quad i = 1, 2, \tag{3}$$

at Γ_1 and Γ_2.

In addition, at the bottom of the melt meniscus ($y = 0$) and at the top of the crystal ($y = 1$) the following temperatures are preset

$$T_1(x, 0) = T_1^0 = \text{constant} \quad -a \leqslant x \leqslant a \tag{4a}$$

$$T_2(x, l) = T_2^0 = \text{constant} \quad -b \leqslant x \leqslant b \tag{4b}$$

The profile curve of the liquid meniscus $f(y)$ should satisfy the Laplace capillary equation

$$\rho_2 g(y + H_0) = \sigma_{LG} \frac{d}{dy}\left[\frac{df/dy}{(1 + [df/dy)^2]^{1/2}}\right], \quad f(0) = a \tag{5}$$

and the joint of the interface boundary of the crystal lateral surface with the meniscus profile curve at the triple point should be related to the meniscus height $H(b)$ by means of the condition related to constancy of the angle of growth

$$-\left.\frac{df}{dy}\right|_{y=H(b)} = tg\,\phi_0 \tag{6}$$

To determine the field of the melt velocities in the meniscus we consider the motion of liquid in the capillary channel, assuming that inside at a distance greater than distance H^* from its edge, this motion is described by the well-known Navier–Stokes equation for the case of flow between two planes. For $V_1 = (u_1, v_1)$ we have the following system of equations and boundary conditions for the above region

$$\mu \Delta V_1 = \frac{\nabla P}{\rho_1} + f \quad f = (0, -g) \tag{7}$$

$$\operatorname{div} V_1 = 0 \tag{8}$$

and

$$V_{1n} = V_0[1 + (H_x')^2]^{1/2} \quad V_{1t} = 0 \tag{9}$$

at the interface boundary $y = H(x)$

$$V_{1n} = 0 \quad [(\tau, DV_1), s] = 0 \tag{10a}$$

on the profile curve of meniscus $x = f(y)$. Here

$$DV_1 = \begin{pmatrix} \dfrac{\partial u_1}{\partial x}, & \dfrac{1}{2}\left(\dfrac{\partial u_1}{\partial y} + \dfrac{\partial v_1}{\partial x}\right) \\ \dfrac{1}{2}\left(\dfrac{\partial u_1}{\partial y} + \dfrac{\partial v_1}{\partial x}\right), & \dfrac{\partial v_1}{\partial x} \end{pmatrix} \tag{10b}$$

is the deformation rate tensor. On the walls of the capillary channel and top surface of the die

$$V_1 = 0 \tag{11}$$

At sufficiently long distance H^* from top of the die, the distribution of melt velocities has the following form

$$u_1 = 0, \; v_1 = \frac{3}{2} V_0 \frac{\rho_2}{\rho_1}\left\{\frac{b}{d}\left[1 - \left(\frac{x}{d}\right)^2\right]\right\} \tag{12}$$

This set of equations and boundary conditions 1–12 define the problem with unknown boundaries $H(x)$ and $f(y)$ for the temperature field in the melt–crystal region and the field of the melt velocities in the meniscus. After it has been solved, the region occupied by the crystal and the distribution of temperature T_2 in it are found. Then the problem of thermoelasticity can be formulated.

Introduce the stress function, F, by the formulas

$$\sigma_x = \frac{\partial^2 F}{\partial y^2}, \quad \sigma_y = \frac{\partial^2 F}{\partial x^2}, \quad \tau_{xy} = -\frac{\partial^2 F}{\partial x \partial y} \tag{13}$$

In the case of plane strain state, F satisfies the relation

$$\Delta^2 F = -\frac{E}{1 - \nu}\alpha_t \Delta T_2 \quad (x, y) \in D_2 \tag{14}$$

The boundary conditions for F are formulated by requiring that there are no surface forces. This can be written out as follows

$$F = 0, \frac{\partial F}{\partial n} = 0 \tag{15}$$

at the crystal boundary. The list of notation is given at the beginning of the paper.

2.2. The finite-element method

Solutions of the Stokes problem and the problem of thermoelasticity in terms of the stream and stress functions, respectively, should satisfy the biharmonic equations. The convenient numerical approach is the finite-element method. While solving the problem of heat transfer it is convenient to use the rectangular elements for approximating the solution [9–11] using the appropriate set of basis functions. However, in typical problems the overall region is not rectangular, and mapping it on to the rectangular leads to the undue complexity of the biharmonic equation and considerable complications in construction of the matrix coefficients of the Galerkin system of equations [12]. Therefore, we use the division of the region into the combined set of rectangles and triangles, as shown in Fig. 1. Hermitian bicubic intrpolating polynomials are used for the rectangles and Birkhoff tricubic polynomials for triangles, respectively [13].

2.3. Numerical analysis

The non-linear system of Galerkin algebraic equations was solved by the Newtonian method, which requires adequate initial approximations. The procedure we have adopted was as follows: first, we fix the convenient value of $b = b_0$ and solve the problem. The solution gives the interface boundary $H(x)$ and the height $H(b)$ of the melt meniscus at the triple point. These data are already sufficient for determining angle ϕ between the generating ribbon and the profile curve of the meniscus at this point. Next we check whether or not the constraint 6 on $\phi(b)$ is fulfilled. The

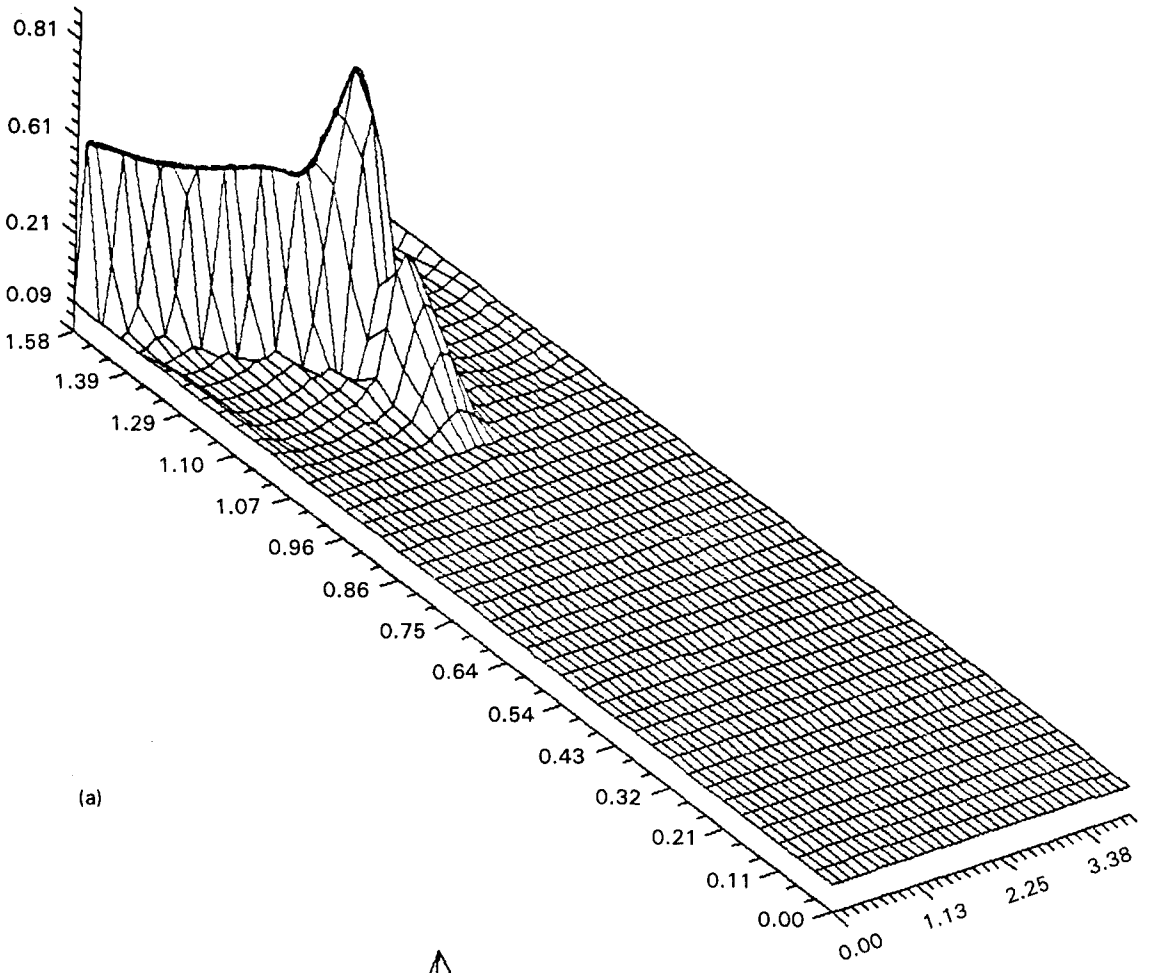

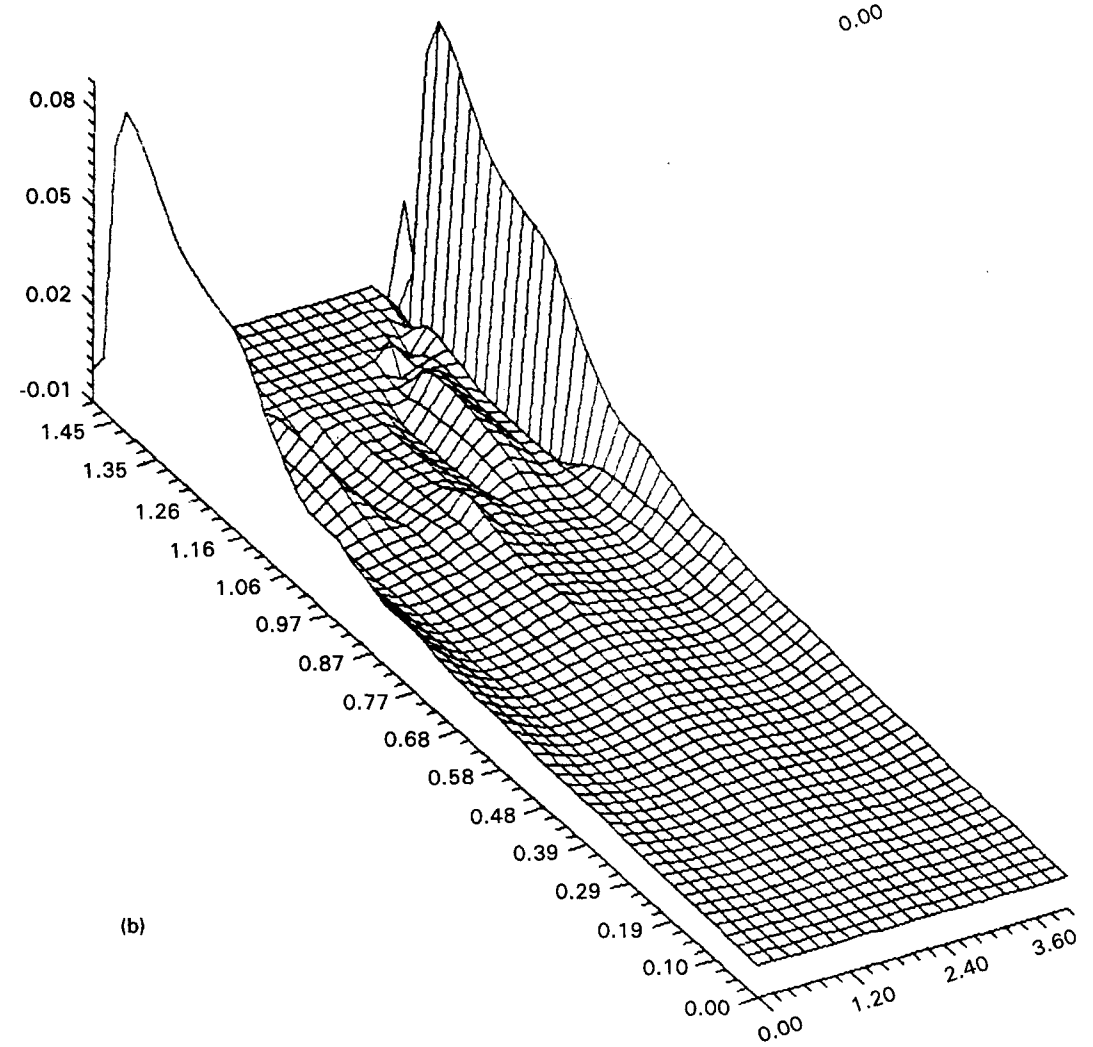

Figure 2 The distributions of thermoelastic stresses: (a) normal stress σ_x, (b) normal stress σ_y, (c) tangential stress τ_{xy}.

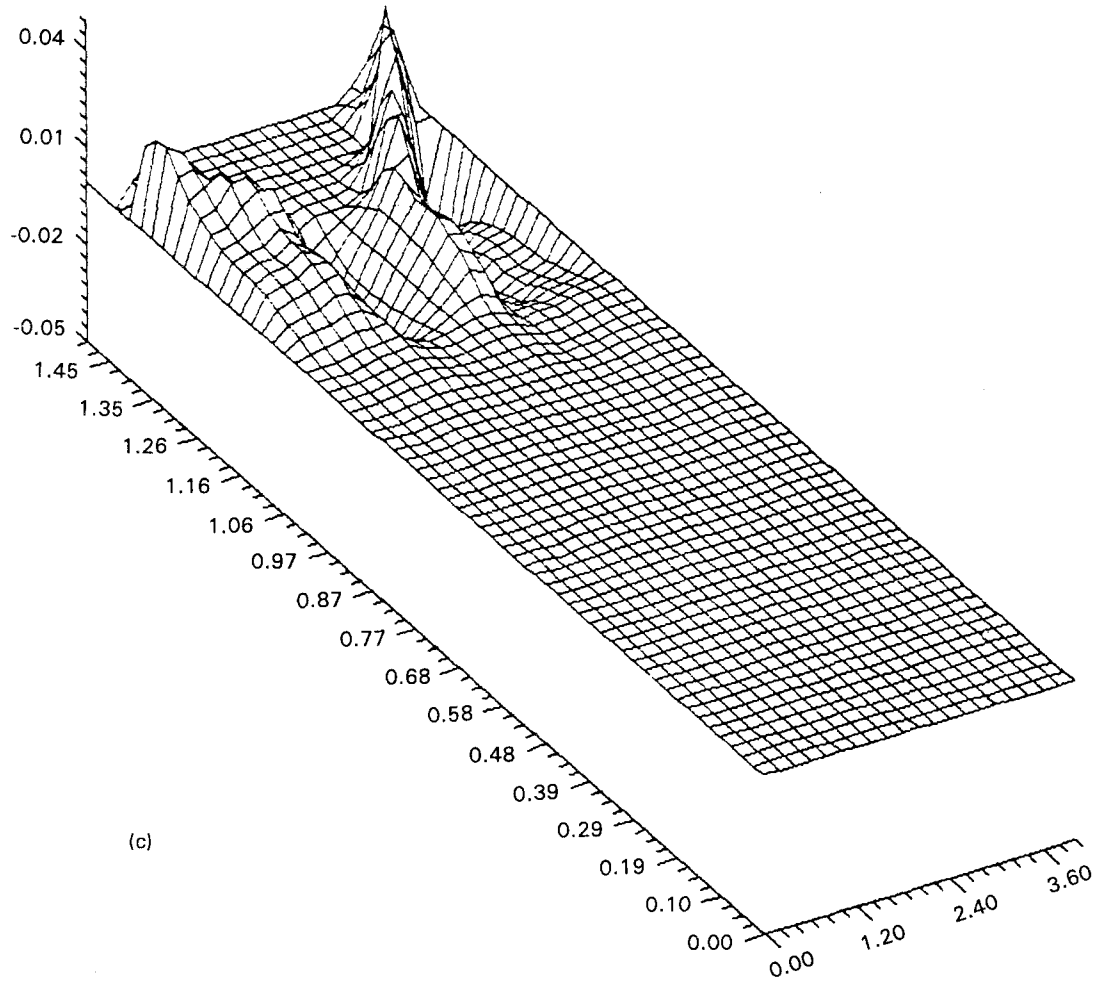

Figure 2c (Continued)

practical procedure is to plot $\phi(b)$ against b and determine the sought half-thickness graphically by drawing the straight line $\phi = \phi_0$ and finding the intersection with the curve $\phi(b)$. This procedure could be quite time consuming. Still another problem is related to the ambiguity. Provided the set (T, D, V) – the temperature, the region occupied by the melt and crystal and melt velocities – represents the solution of Problems 1–12, then under various physical parameters no solution, or two solutions, or three solutions exist, which satisfy all the conditions of the problem formulated.

The choice of the actual value of b should be made on the basis of studying the stability of the crystallization process. In any case we believe b to be found and region D^2, occupied by the crystal, determined. The stress function F is found in the manner described in Section 1.2.

Using Formula 13 we calculate then normal and tangent stresses σ_x, σ_y, τ_{xy}. Fig. 2 shows the surface of stresses determined over the calculation region. It is seen that stresses are concentrated at the crystallization front and on the lateral surface of the ribbon. Normal stress, σ_x is maximum at the centre of the ribbon in the crystallization front and drops drastically towards the upper end of the crystal. The maximal value of normal stress at $b = 1$ mm under the standard growth conditions in the order of 70 MPa. Normal stress, σ_y, is maximum on the lateral surface of the ribbon near the crystallization front, and by an order of magnitude less than the maximal value of σ_x.

The tangential stress is maximum at some distance from the crystallization front, and its magnitude is in the order of maximal σ_y. In the case of plane deformation there also arises normal stress σ_z, associated with the stresses along other axes

$$\sigma_z = \nu(\sigma_x + \sigma_y) - \alpha_t E T_2 \tag{16}$$

Because the top surface of a crystal is free of stresses, then, according to the St Venant condition, thermal stress in the axial direction is determined by the relation

$$\sigma_z' = E\varepsilon_z + \sigma_z \tag{17}$$

Here ε_z is the constant longitudinal strain. Strain ε_z is chosen so that the resultant of the stresses σ_z' acting on the top of the crystal should turn to zero. It is evaluated from

$$\varepsilon_z = -\frac{1}{E|D_2|}\int_{D_2} \sigma_z dx dy \tag{18}$$

Here $|D_2|$ is the area of region D_2.

3. Thermoelastic stresses in tubes

3.1. Mathematical model

We consider the process of crystallization from the melt involving obtaining tubes of inner radius R_1 and

outer radius R_2. The pulling rate, V_0, and the temperature regime of the thermal unit are assumed to be known from experimental data. Owing to the smallness of the pulling rate the problem concerned with the determination of the temperature field in the crystal will be considered in the quasi-stationary approximation. We introduce the cylindrical system of coordinates r, z of which the z-axis is directed along the symmetry axis of the tube and its origin is the centre of the lower tube end. Then, the temperature T satisfies the following thermal conduction equation

$$k_2 \Delta T - V_0 \rho_2 c_{ps} \frac{\partial T}{\partial z} = 0 \tag{19}$$

At the inner ($r = R_1$) and outer ($r = R_2$) lateral surface we preset the heat exchange with the ambient environments having the temperatures Θ_1 and Θ_2

$$k_2 \frac{\partial T}{\partial r} = h_2(T - \Theta_1)\Big|_{r=R_1}, \qquad -k_2 \frac{\partial T}{\partial r} = h_2(T - \Theta_2)\Big|_{r=R_2} \tag{20}$$

where

$$\Theta_1 = \begin{cases} T_1^0 + \frac{z}{l^*}(T_2^0 - T_1^0), & 0 \leqslant z \leqslant l^* \\ \frac{T_5^0 - T_2^0}{l - l^*} z + \frac{T_2^0 l - T_5^0 l^*}{l - l^*}, & l^* \leqslant z \leqslant l \end{cases} \tag{21a}$$

$$\Theta_2 = \begin{cases} T_3^0 + \frac{z}{l^*}(T_4^0 - T_3^0), & 0 \leqslant z \leqslant l^* \\ \frac{T_6^0 - T_4^0}{l - l^*} z + \frac{T_4^0 l - T_6^0 l^*}{l - l^*}, & l^* \leqslant z \leqslant l \end{cases} \tag{21b}$$

Here l^* is the screen height, and T_1^0 and T_3^0 are the ambient temperatures inside and outside the tube at $z = 0$, analogously T_5^0, T_6^0 and T_2^0, T_4^0 are the ambient temperatures at $z = l^*$ and $z = l$, respectively. These temperatures can be directly measured in the process of the crystal growth. So, the ambient temperatures are preset by the piecewise linear functions. Besides, at the solid–liquid interface $z = 0$ and at the upper tube end $z = l$ the temperatures

$$T(r, 0) = T_m, \quad T(r, l) = T_0, \quad R_1 \leqslant r \leqslant R_2 \tag{22}$$

are given.

The solution of Problems 19–22 is given as the sum

$$T(r, z) = T^*(r, z) + T_1(r, z) \tag{23}$$

where the T^* function is such that it satisfies the boundary conditions only

$$k_2 \frac{\partial T^*}{\partial r} = h_2(T^* - \Theta_1)\Big|_{r=R_1}, \qquad -k_2 \frac{\partial T^*}{\partial r} = h_2(T^* - \Theta_2)\Big|_{r=R_2} \tag{24}$$

This function that also satisfies the equation $\Delta T^* = 0$ may be written as

$$T^*(r, z) = A(z) \ln r + C(z) \tag{25}$$

where the coefficients $A(z)$ and $C(z)$ have the form

$$A(z) = \lambda \frac{\Theta_2 - \Theta_1}{w_1 + w_2}, \quad C(z) = \frac{\Theta_1 w_2 + \Theta_2 w_1}{w_1 + w_2} \tag{26a}$$

$$w_1 = \frac{1}{R_1} - \lambda \ln R_1, \quad w_2 = \frac{1}{R_2} + \lambda \ln R_2, \quad \lambda = \frac{h_2}{k_2} \tag{26b}$$

For temperature T_1 we shall then have a thermal conduction equation, but with uniform boundary conditions at the inner and outer tube lateral surfaces. To determine T_1, a method of variables separation is applicable according to which the T_1 solution is given as

$$T_1(r, z) = \sum_{k=1}^{\infty} Z_k(z) X_k(r) \tag{27}$$

Here functions $X_k(r)$ are determined by equalities

$$X_k = \frac{D_k(r)}{\|D_k\|}, \quad D_k = D\left(\frac{\mu_k}{R_2} r\right) = J_0\left(\frac{\mu_k}{R_2} r\right) + \gamma(\mu_k) N_0\left(\frac{\mu_k}{R_2} r\right) \tag{28}$$

where J_0, N_0 are zeros of first and second order Bessel functions, respectively.

The eigenvalues, μ_k, are the solutions of the algebraic equation

$$\begin{vmatrix} \mu J_1(\mu) - \kappa J_0(\mu), & \mu N_1(\mu) - \kappa N_0(\mu) \\ \mu J_1\left(\mu \frac{R_1}{R_2}\right) + \kappa J_0\left(\mu \frac{R_1}{R_2}\right), & \mu N_1\left(\mu \frac{R_1}{R_2}\right) + \kappa N_0\left(\mu \frac{R_1}{R_2}\right) \end{vmatrix} = 0 \tag{29}$$

and the coefficients $\gamma(\mu_k)$ are equal to

$$\gamma(\mu_k) = -\frac{\mu_k J_1(\mu_k) - \kappa J_0(\mu_k)}{\mu_k N_1(\mu_k) - \kappa N_0(\mu_k)} \tag{30}$$

The square of the norm of functions D_k equals

$$\|D_k\|^2 = \frac{(\kappa^2 + \mu_k^2)}{2\lambda_k}\left[D^2(\mu_k) - \left(\frac{R_1}{R_2}\right)^2 D^2\left(\mu_k \frac{R_1}{R_2}\right)\right], \quad \kappa = \frac{\lambda}{R_2} \tag{31}$$

The functions Z_k satisfy the differential equation

$$Z_k'' - \chi Z_k' - \lambda_k Z_k = C_k, \quad \lambda_k = \left(\frac{\mu_k}{R_2}\right)^2, \quad \chi = \frac{V_0 \rho_2 c_{ps}}{k_2} \tag{32}$$

with boundary conditions

$$Z_k(0) = (T_m - T^*(0), X_k)_\rho = a_k,$$
$$Z_k(l) = (T_0 - T^*(l), X_k)_\rho = b_k \quad (33)$$

By $(\cdot,\cdot)_\rho$ we designate the scalar product in the space $L_2^\rho(0, l)$ with weight $\rho = r$. The righthand parts of Equation 32 C_k have the form

$$C_k = -C_k^{(3)}\delta(z - l^*) + \begin{cases} C_k^{(1)} & \text{if } z \leqslant l^* \\ C_k^{(2)} & \text{if } z > l^* \end{cases} \quad (34)$$

where $\delta(z)$ is the Dirac delta function.

$$C_k^{(i)} = \frac{\chi}{\|D_k\|\lambda_k}\left\{[\alpha_i(\kappa \ln R_2 + 1) + \kappa\beta_i]D(\mu_k) + \left[\alpha_i\left(\kappa\frac{R_1}{R_2}\ln R_1 - 1\right) + \beta_i\kappa\frac{R_1}{R_2}\right]\right\}D\left(\mu_k\frac{R_1}{R_2}\right),$$
$$i = 1, 2 \quad (35)$$

$$\alpha_1 = \lambda\frac{T_4^0 + T_1^0 - T_2^0 - T_3^0}{l^*(w_1 + w_2)},$$
$$\beta_1 = \frac{(T_2^0 - T_1^0)w_2 + (T_4^0 - T_3^0)w_1}{l^*(w_1 + w_2)} \quad (36a)$$

$$\alpha_2 = \lambda\frac{T_6^0 + T_2^0 - T_4^0 - T_5^0}{(l - l^*)(w_1 + w_2)},$$
$$\beta_2 = \frac{(T_5^0 - T_2^0)w_2 + (T_6^0 - T_4^0)w_1}{(l - l^*)(w_1 + w_2)} \quad (36b)$$

Coefficients $C_k^{(3)}$ are calculated according to Formula 35, only instead of α_i one has to take $(\alpha_2 - \alpha_1)$ and instead of β_i, $(\beta_2 - \beta_1)$, and the value of χ should be equal to 1. The boundary values a_k and b_k are calculated in implicit form and equal to

$$a_k = \frac{1}{\|D_k\|\lambda_k}\left\{\kappa\delta_1\left[D(\mu_k) + \frac{R_1}{R_2}D\left(\mu_k\frac{R_1}{R_2}\right)\right] + \gamma_1\left[\kappa D(\mu_k)\ln R_2 + \kappa\frac{R_1}{R_2}D\left(\mu_k\frac{R_1}{R_2}\right)\ln R_1 + D(\mu_k) - D\left(\mu_k\frac{R_1}{R_2}\right)\right]\right\} \quad (37)$$

where

$$\delta_1 = T_m - \frac{T_1^0 w_2 + T_3^0 w_1}{w_1 + w_2},$$
$$\gamma_1 = -\lambda\frac{T_3^0 - T_1^0}{w_1 + w_2} \quad (38)$$

Coefficients b_k are calculated from the same formulas as a_k, only instead of δ_1 and γ_1 one has to take δ_2 and γ_2. Quantities δ_2 and γ_2 are calculated from the formulas

$$\delta_2 = T_0 - \frac{T_5^0 w_2 + T_6^0 w_1}{w_1 + w_2}, \quad \gamma_2 = -\lambda\frac{T_6^0 - T_5^0}{w_1 + w_2} \quad (39)$$

And finally, the functions $Z_k(z)$ using the above accepted symbols, should be written as

$$Z_k(z) = Z_k^{(0)} - Z_k^{(1)} + C_k^{(3)}G_k(z, l^*) \quad (40a)$$

$$Z_k^{(0)} = a_k\left[\exp\chi z/2 sh\frac{\eta_k(l - z)}{2}\Big/\left(sh\frac{\eta_k l}{2}\right)\right] + b_k\left[\exp\frac{\chi(z - l)}{2}sh\frac{\eta_k z}{2}\Big/\left(sh\frac{\eta_k l}{2}\right)\right],$$
$$\eta_k = (\chi^2 + 4\lambda_k)^{1/2} \quad (40b)$$

$$G_k(z, l^*) = \left[2\exp\frac{\chi(z - l^*)}{2}\Big/\left(\eta_k sh\frac{\eta_k l}{2}\right)\right] \times \begin{cases} sh\frac{\eta_k z}{2}sh\frac{\eta_k(l - l^*)}{2} & z \leqslant l^* \\ sh\frac{\eta_k(l - z)}{2}sh\frac{\eta_k l^*}{2} & z > l^* \end{cases} \quad (40c)$$

and $Z_k^{(1)}$ is equal to

$$Z_k^{(1)} = \left[\exp\frac{\chi z}{2}\Big/\left(\lambda_k sh\frac{\eta_k l}{2}\right)\right]\left\{sh\frac{\eta_k(l - z)}{2} \times\left[\exp\left(-\frac{\chi z}{2}\right)\left(\frac{\chi}{\eta_k}sh\frac{\eta_k z}{2} + ch\frac{\eta_k z}{2}\right) - 1\right]\right\} \times C_k^{(1)} + sh\frac{\eta_k z}{2}\left\{\exp\frac{-\chi l^*}{2}\left[\frac{\chi}{\eta_k}sh\frac{\eta_k(l - l^*)}{2} - ch\frac{\eta_k(l - l^*)}{2}\right] - \exp\frac{-\chi z}{2}\left[\frac{\chi}{\eta_k}\,sh\,\frac{\eta_k(l - z)}{2} - ch\frac{\eta_k(l - z)}{2}\right]\right\}C_k^{(1)} - sh\frac{\eta_k z}{2}\left\{\exp\left(\frac{-\chi l^*}{2}\right) \times\left[\frac{\chi}{\eta_k}sh\frac{\eta_k(l - l^*)}{2} - ch\frac{\eta_k(l - l^*)}{2}\right] + \exp\left(\frac{-\chi l}{2}\right)\right\}C_k^{(2)}\Bigg], \quad z \leqslant l^* \quad (41a)$$

$$Z_k^{(1)} = \left[\exp\frac{\chi z}{2}\Big/\left(\lambda_k sh\frac{\eta_k l}{2}\right)\right]\left(sh\frac{\eta_k(l - z)}{2} \times\left[\exp - \frac{\chi l^*}{2}\left(\frac{\chi}{\eta_k}sh\frac{\eta_k l^*}{2} + ch\frac{\eta_k l^*}{2}\right) - 1\right]\cdot C_k^{(1)} + sh\frac{\eta_k(l - z)}{2}\left[\exp\frac{-\chi z}{2}\left(\frac{\chi}{\eta_k}sh\frac{\eta_k z}{2} + ch\frac{\eta_k z}{2}\right) + \exp\frac{-\chi l^*}{2}\left(\frac{\chi}{\eta_k}sh\frac{\eta_k l^*}{2} + ch\frac{\eta_k l^*}{2}\right)\right]\cdot C_k^{(2)} - sh\frac{\eta_k z}{2}\left\{\exp\left(\frac{-\chi z}{2}\right)\left[\frac{\chi}{\eta_k}sh\frac{\eta_k(l - z)}{2} - ch\frac{\eta_k(l - z)}{2}\right] + \exp\frac{-\chi l}{2}\right\}\cdot C_k^{(2)}\Bigg), \times z > l^*. \quad (41b)$$

In order to calculate the thermoelastic stress-deformed state we represent the tube as a circular cylindrical shell of a constant thickness. We designate the shell thickness as $h = R_2 - R_1$, $R = (R_1 + R_2)/2$ is the middle surface radius, u, ω are axial and radial displacements of the middle surface, respectively, and σ_m and σ_ϕ are meridianal and radial normal stresses.

The thermal stresses σ_m and σ_ϕ are determined from the well-known equations [7]

$$\sigma_m = \frac{E}{1-\nu^2}\left[\frac{du}{dz} - x\frac{d^2\omega}{dz^2} + \nu\frac{\omega}{R} - (1+\nu)\alpha_t T\right] \quad (42a)$$

$$\sigma_\phi = \frac{E}{1-\nu^2}\left[\nu\frac{du}{dz} - \nu x\frac{d^2\omega}{dz^2} + \frac{\omega}{R} - (1+\nu)\alpha_t T\right] \quad (42b)$$

$$u = \int\left[(1+\nu)\bar{T} - \nu\frac{\omega}{R}\right]dz,$$

$$M = -D\left[\frac{d^2\omega}{dz^2} + (1+\nu)\alpha_t\bar{T}\right] \quad (42c)$$

The value x in Equations (42) is measured from the tube middle surface ($-0.5h \leqslant x \leqslant 0.5h$).

The components of the displacement vector ω satisfy the equation

$$\frac{d^4\omega}{dz^4} + 4k^4\omega = \frac{Eh\alpha_t}{DR}\bar{T} - (1+\nu)\alpha_t\frac{d^2\bar{\bar{T}}}{dz^2} \quad (43a)$$

$$\bar{T} = \frac{1}{h}\int_{-h/2}^{h/2} T(R+x,z)\,dx,$$

$$\bar{\bar{T}} = \frac{12}{h^3}\int_{-h/2}^{h/2} T(R+x,z)\,x\,dx \quad (43b)$$

The boundary conditions for Equations 43 are formulated for a shell having free edges, i.e.

$$M = \frac{dM}{dz} = 0, \quad z = 0, l \quad (44)$$

In Equations 42 and 43, through k, D, we designate

$$k^4 = \frac{3(1-\nu^2)}{h^2R^2}, \quad D = \frac{E\cdot h^3}{12(1-\nu^2)}$$

The materials characteristics and the process parameters are tabulated elsewhere [14–16]. It should be noted that the chosen heat-transfer coefficient allows for the overall heat transfer by emission and convection.

3.2. Numerical analysis

A typical distribution of the meridianal σ_m and circular σ_ϕ normal stresses in the longitudinal tube section are shown in Figs 4 and 5. The grown tube length was $l = 15$ cm, the screen height was $l^* = 8$ cm. For clarity the same figures show stresses in the tubes at the same ambient temperatures near the liquid–solid interface T_1^0, T_3^0 and near the upper tube end T_5^0, T_6^0, but in the absence of the screen. As seen from the figures the presence of the screen gives rise to a "peak" of stresses that drops rapidly as the distance from l^* grows. Although the stress near l^* may be significant, the maximal stress values in this case diminish approximately two-fold.

A further analysis of the stress behaviour as a function of the heat-transfer conditions, tube thickness and magnitude of the middle radius will be conducted for the tube placed completely in the screen zone. An increase of the heat transfer naturally increases

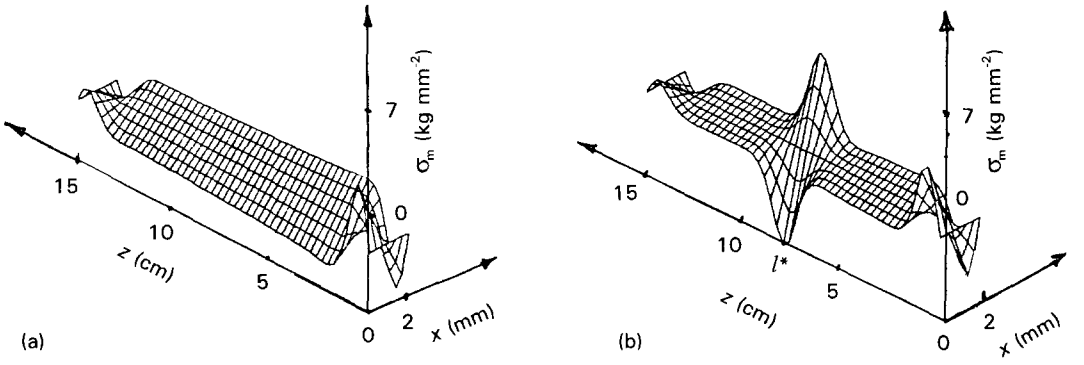

Figure 3 Typical distribution of the normal meridianal stress σ_m: (a) without a screen, (b) with a screen.

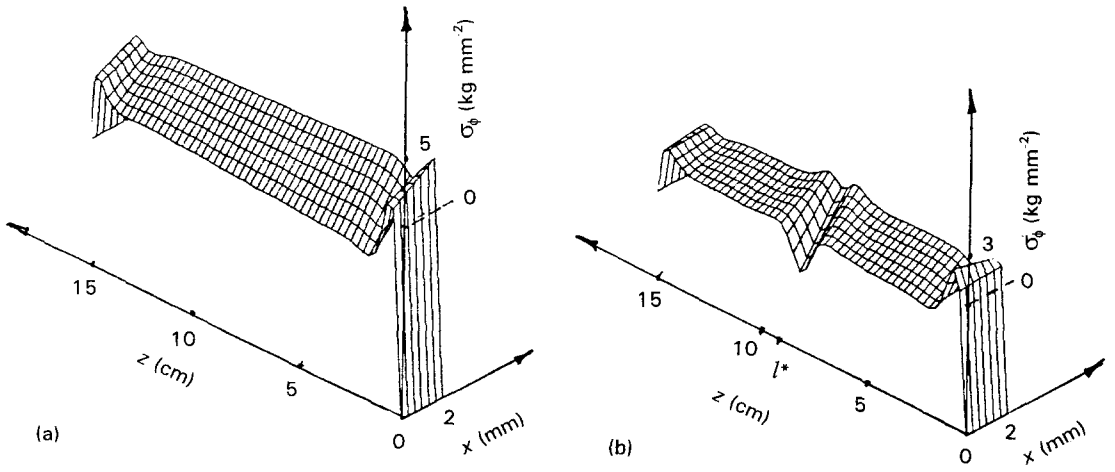

Figure 4 Typical distribution of the normal circular stress σ_ϕ: (a) without a screen, (b) with a screen.

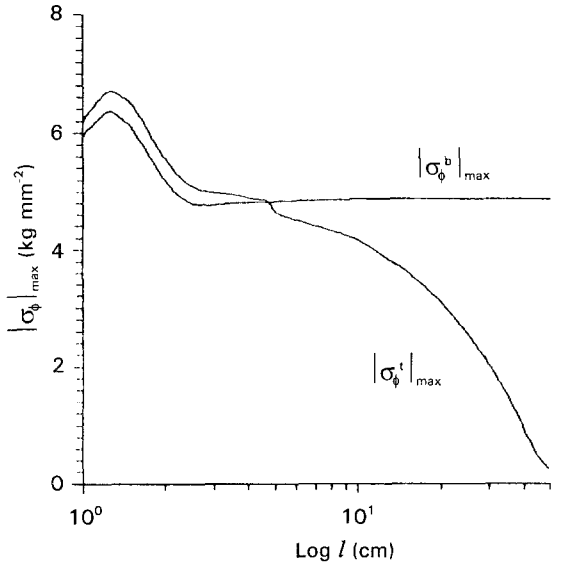

Figure 5 Dependence of $|\sigma_\phi|_{max}$ on the crystal length.

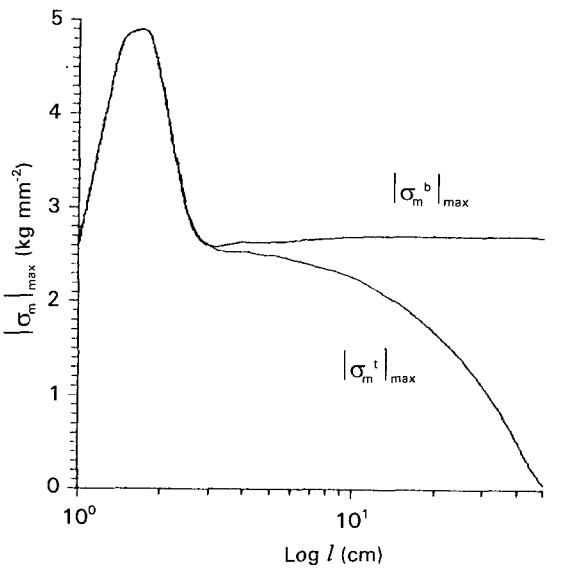

Figure 6 Dependence of $|\sigma_m|_{max}$ on the crystal length.

the temperature variations on the tube wall. Near the liquid–solid interface at $T_1^0 = 2000\,^\circ C$ and $T_3^0 = 1950\,^\circ C$ the radial temperature gradients do not exceed $10–15\,^\circ C\,cm^{-1}$. At $T_1^0 = 1900\,^\circ C$ and $T_3^0 = 1700\,^\circ C$ the radial temperature gradients reach $70\,^\circ C\,cm^{-1}$. Accordingly, maximal circular stresses at the lower crystal end (liquid–solid interface) amount to $|\sigma_\phi| = 5.12$ and 16.4 kg mm^{-2} for a 5 cm long tube in either case. Near the liquid–solid interface there are small regions where normal stresses σ_ϕ change rapidly from the negative to the positive values and after that they decrease down to close-to-zero values, remaining virtually such throughout the tube length.

The largest $|\sigma_\phi|$ stress values are achieved at the crystal ends, and largest $|\sigma_m|$ values near the ends on the tube surface; their behaviour will be considered.

We designate the maximal $|\sigma_\phi|$ value at the liquid–solid interface as $|\sigma_\phi^b|_{max}$ that at the upper tube end as $|\sigma_\phi^t|_{max}$, $|\sigma_m^b|_{max}$ and $|\sigma_m^t|_{max}$ are the maximal $|\sigma_m|$ values near the lower and upper tube ends, respectively.

Figs 5 and 6 depict the dependences of $|\sigma_\phi^b|_{max}$, $|\sigma_\phi^t|_{max}$, $|\sigma_m^b|_{max}$, $|\sigma_m^t|_{max}$ on the growing crystal length. The presented plots suggest that starting from a certain length (3.5 cm) the $|\sigma_\phi^b|_{max}$ and $|\sigma_m^b|_{max}$ are nearly constant, and $|\sigma_\phi^t|_{max}$, $|\sigma_m^t|_{max}$ rapidly decrease. On a small length (up to 3.5 cm) there are portions of a drastic increase and decrease of all the stresses, their magnitudes being not smaller than on lengths larger than 3.5 cm. Therefore, at the initial growth stage when the crystal is not long the influence of the σ_ϕ^t and σ_m^t stresses near the upper end is essential for the crystal structure formation. With a tube elongation these stresses are relieved and, starting from a certain length, the influence of these stresses on the crystal structure will be insignificant. Consequently, the conditions of formation of the dislocation structure (with allowance for polygonization) and the block structure in the tubes, grown from a small seed rod and grown from a long tubular seed crystal of the same diameter as the obtained sample, are significantly different. These results suggest the conclusion that when growing a tube it is better to start with a tubular seed not shorter than a certain value (in our particular case, 3.5 cm).

We have followed the $|\sigma_\phi|_{max}$ and $|\sigma_m|_{max}$ dependences on the middle tube radius, R, at a constant wall thickness, h. It was found that on increasing the radius, a significant increase in the $|\sigma_\phi|_{max}$ stress resulted, a change in $|\sigma_m|_{max}$ being insignificant in this case.

We have also studied the dependences of these stresses on the wall thickness h with a constant R. The calculations have shown that $|\sigma_\phi|_{max}$ and $|\sigma_m|_{max}$ stresses decrease monotonically with the growing tube wall thickness.

The calculation of the stresses carried out is based on the experimentally determined values of $\Theta_1(z)$ and $\Theta_2(z)$. Moreover, by varying these dependences, one may determine the optimal temperature distribution along the furnace in order to obtain the minimal stresses in the tube at heat transfer sufficient for accomplishing the crystallization process.

4. Conclusions

1. Several different solutions may exist satisfying all the conditions of the Stefan problem formulated for the ribbon case. The choice of the actual solution should be made on the basis of studying the stability of the crystallization process.

2. Normal stress, σ_x, in the ribbons is maximal at the centre on the interface boundary and drops drastically in the direction of the upper end of the crystal and, in addition, its maximal value is by an order of magnitude greater than maximal values σ_y, τ_{xy}.

3. The behaviour of the thermoelastic stresses is appreciably different for growing the crystal on to a small seed rod or a long tubular seed whose dimension complies with the growing crystal. To grow a tube it is more advantageous to use a tubular seed of the appropriate length.

4. An increase in the heat transfer from the tube surface causes an increase in the maximal circular and meridianal stresses.

5. As the length of the growing tube increases, the circular stress at the liquid–solid interface and the maximal meridianal stress near the liquid–solid interface, become stabilized.

6. As the wall thickness is increased, the maximal values of the circular and meridianal stresses are lowered. An increase in the tube diameter with a constant wall thickness causes an increase in the circular stress and does not practically change the meridianal stress.

References

1. A. S. JORDAN, A. R. VON NEIDA and R. CARUSO, *Bell System Tech. J.* **59** (1980) 593.
2. S. MOTAKEF and A. F. WITT, *J. Crystal Growth* **80**(1987) 37.
3. H. ALEXANDER and P. HAASEN, *Solid State Phys.* **22** (1968) 27.
4. D. MAROUDAS and R. A. BROWN, *J. Crystal Growth* **108** (1991) 399.
5. S. MOTAKEF, *ibid.* **114** (1991) 47.
6. D. E. BORNSIDE, T. A. KINNEY and R. A. BROWN, *ibid.* **108** (1991) 779.
7. J. LAMBROPOULOS, *ibid.* **104** (1990) 1.
8. P. I. ANTONOV, V. M. KRYMOV and V. S. JUFEREV, in "The 7th All-Union Conference on Crystal Growth", Nauka, Moscow, edited by A. A. Chemov (1988) pp. 26–7.
9. J. P. KALEJS, L.-Y. CHIN, and F. M. CARLSON, *J. Crystal Growth* **61** (1983) 473.
10. P. D. THOMAS, H. M. ETTOUNEY and R. A. BROWN, *ibid.* **76** (1986) 339.
11. J. J. DERBY, and R. A. BROWN, *ibid.* **87** (1988) 251.
12. C. A. J. ELETCHER, "Computational Galerkin Methods" (Springer, New York, Berlin, Heidelberg, Tokyo, 1984).
13. A. R. MITCHELL and R. WAIT, "The Finite-Element Method In Partial Differential Equations" (Wiley, Chichester, New York, Brisbane, Toronto, 1977).
14. S. V. ARTEMOV, I. V. ALJABJEEV and V. S. PAPKOV, *Izv. An. SSSR, Ser. Phys.* **52** (1988) 1977.
15. M. V. KLASSEN-NEKLIUDOVA and Kh. S. BAGDASAROV (eds) "Ruby and Sapphire" (Nauka, Moscow, 1974) p. 236 (in Russian).
16. G. V. SAMSONOV (ed.) "Physical-chemical properties of the oxides. Handbook" (Metallurgija, Moscow, 1978) 472 pp. (in Russian).

Received 7 January
and accepted 5 May 1994